Hydrogen dissociation on metal surfaces: A semi-empirical approach

Nour Ghassemi, E.

CHAPTER 6

Assessment of Two Problems of Specific Reaction Parameter Density Functional Theory : Sticking and Diffraction of H_2 on Pt(111)

This chapter is based on:

Elham Nour Ghassemi, Mark F. Somers, and Geert-Jan Kroes The Journal of Physical Chemistry C **123**(16), 10406-10418, 2019.

Abstract

It is important that theory is able to accurately describe dissociative chemisorption reactions on metal surfaces, as such reactions are often rate controlling in heterogeneously catalyzed processes. Chemically accurate theoretical descriptions have recently been obtained on the basis of the specific reaction parameter (SRP) approach to density functional theory (DFT), allowing reaction barriers to be obtained with chemical accuracy. However, being semi-empirical this approach suffers from two basic problems. The first is that sticking probabilities (to which SRP density functionals (DFs) are usually fitted) might show differences across experiments, of which the origins are not always clear. The second is that it has proven hard to use experiments on diffractive scattering of H_2 from metals for validation purposes, as dynamics calculations using a SRP−DF may yield a rather poor description of the measured data, especially if the potential used contains a van der Waals well. We address the first problem by performing dynamics calculations on three sets of molecular beam experiments on D_2 + Pt(111), using four sets of molecular beam parameters to obtain sticking probabilities, and the SRP−DF recently fitted to one set of experiments on D_2 + Pt(111). It is possible to reproduce all three sets of experiments with chemical accuracy with the aid of two sets of molecular beam parameters. The theoretical simulations with the four different sets of beam parameters allow one to determine for which range of incidence conditions the experiments should agree well, and for which conditions they should show specific differences. This allows one to arrive at conclusions about the quality of the experiments, and about problems that might affect the experiments. Our calculations on diffraction of H_2 scattering from Pt(111) show both quantitative and qualitative differences with previously measured diffraction probabilities, which were Debye-Waller (DW) extrapolated to 0 K. We suggest that DW extrapolation, which is appropriate for direct scattering, might fail if the scattering is affected by the presence of a van der Waals well, and that theory should attempt to model surface atom motion for reproducing diffraction experiments performed for surface temperatures of 500 K and higher.

6.1 Introduction

Dissociative chemisorption reactions are important elementary surface reactions, in the sense that they often control the rate of heterogeneously catalyzed processes [1, 2], which are used in most of the reactive processes carried out by the chemical industry [3]. Well-known examples include N_2 dissociation in ammonia synthesis [4] and the dissociative chemisorption of methane in the steam reforming reaction [5]. Simulating rate-controlling reactions accurately is crucial to the calculation of accurate rates of the overall catalyzed processes [6]. Therefore, it is important to be able to perform accurate calculations on dissociative chemisorption reactions.

At present, the best method to obtain accurate results (and in some cases predictions) for dissociative chemisorption reactions is based on a semi-empirical version of density functional theory, called the specific reaction parameter (SRP) approach to DFT (SRP−DFT). This method has now been applied successfully to three H_2-metal systems (H_2 + Cu(111) [7], H_2 + Cu(100) [8], and H_2 + Pt(111) [9]), and three CH_4-metal systems (CHD_3 + Ni(111) [10], CHD_3 + Pt(111) [11], and CHD_3 + Pt(211) [11]). The method is predictive to the extent that it is often possible to derive an accurate SRP density functional (SRP−DF) by simply taking the SRP−DF from a chemically related system: the SRP−DF for H_2 + Cu(111) accurate describes the dissociation of H_2 on Cu(100) [8], and the SRP−DF for CH_4 + Ni(111) accurately describes CHD_3 + Pt(111) and Pt(211) [11].

However, being semi-empirical and in need of validation, the SRP−DFT approach is not without problems. The first problem is that the SRP−DFT approach is obviously no more accurate than the underlying experimental data are. This problem can become severe if different sets of measurements of the sticking probability for a specific system show widely differing results, as recently explored for H_2 + Pd(111) [12]. The second problem has to do with the demands put on SRP−DFs. For a density functional to be called a SRP−DF, a requirement put forward is that at least one set of experiments not used to derive the SRP−DF can be accurately reproduced with dynamics calculations based on that SRP−DF. This has recently been a problem for H_2 + Ru(0001), where it was possible to accurately reproduce sticking experiments, but not diffraction experiments, with dynamics calculations based on two functionals also containing van der Waals correlation [13].

Here we address the above two problems for the dissociative chemisorption of deuterated dihydrogen on Pt(111). Platinum is an important hydro-

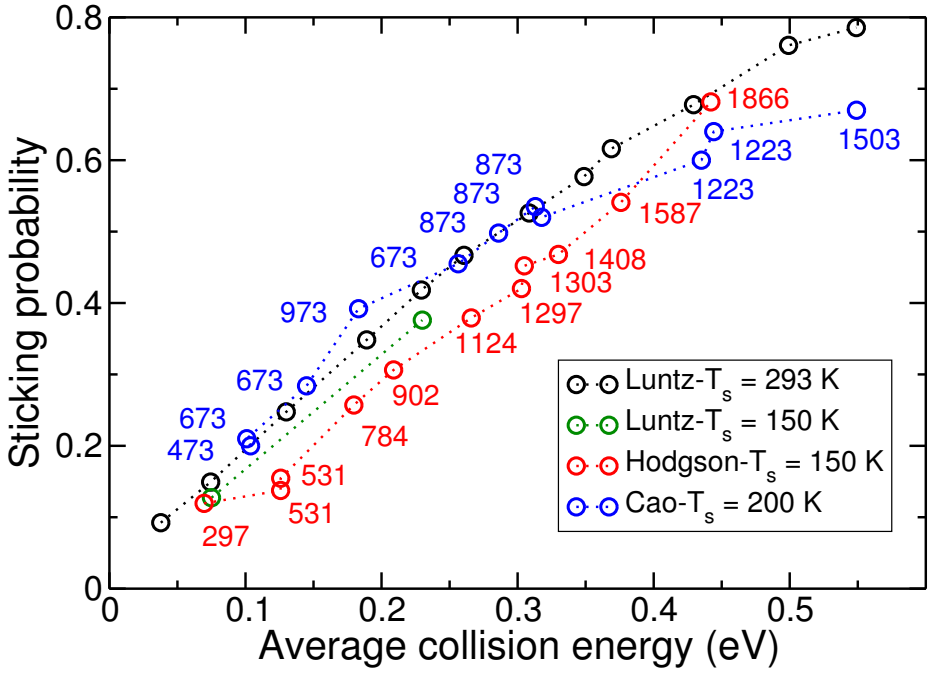

Figure 6.1: Comparison of the energy dependence of the sticking probability of D_2 on Pt(111) for three different sets of experimental data from Hodgson and co-workers [16] (red circles), Luntz *et al.* [15] (black circles for a surface temperature T_s of 293 K, green circles for $T_s \approx 150$ K), and Cao *et al.* [17] (blue circles). Nozzle temperatures T_n are indicated (in K) for the experiments of Hodgson and co-workers and of Cao *et al.*.

genation catalyst [14], and consequently the sticking of H_2 on Pt(111) has been studied in molecular beam experiments by three different groups [15–17]. While the outcome of these experiments is not as varied as results for H_2 + Pd(111), as discussed further below there are nevertheless considerable differences between the sets of sticking probabilities S_0 measured in the three experiments (see also Figure 6.1).

Diffractive scattering of dihydrogen from Pt surfaces has been studied experimentally by Cowin *et al.* in the 1980s [18–20], and more recently by Nieto *et al.* who also looked at out-of-plane diffraction [21]. An SRP−DF for H_2 + Pt(111) [9] has been fitted to molecular beam experiments on stick-

ing at normal incidence [15], and validated against sticking measurements performed for off-normal incidence [15].

Several theoretical studies have addressed the reactive [9, 21–28] and the diffractive [21, 22, 25, 26] scattering of dihydrogen from Pt(111). Dynamics calculations based on the B88P86 generalized gradient approximation (GGA) exchange-correlation (XC) functional [29, 30] were able to reproduce measured sticking probabilities and in-plane and out-of-plane diffraction probabilities semi-quantitatively [21]. This might be taken to suggest that an SRP−DF can be fitted to molecular beam experiments on sticking, and then validated by showing that, on the basis of the fitted SRP−DF, diffraction probabilities can be reproduced quantitatively. However, calculations on H_2 + Ru(0001) have shown that this may be problematic [13], although for this case the situation could be improved by assuming static disorder of the surface [31]. Furthermore, comparisons of quantum dynamics (QD) calculations and quasi-classical trajectory (QCT) calculations modeling motion in all six degrees of freedom (DOFs) of H_2 have established that the reaction of ($\nu = 0$, $j = 0$) H_2 [24] and of ($\nu = 0$, $j = 0$) D_2 [9] can be accurately modeled with the QCT method. Finally, QD calculations on H_2 + Pt(111) [27] and QCT calculations on D_2 + Pt(111) [9] have suggested that in the simulation of S_0 measured in molecular beam experiments it should already be a good approximation to simply compute the reaction probability for ($\nu = 0$, $j = 0$) dihydrogen at the average incident energy $\langle E_i \rangle$, and to omit the averaging over the translational energy distribution and the rovibrational energy distribution of H_2 in the beam. Here, ν and j are the vibrational and rotational quantum numbers of H_2.

Here, we use the recently determined SRP−DF for D_2 + Pt(111) to simulate all three available sets of S_0 measured in supersonic molecular beam experiments with QCT calculations. The question we address is whether it is possible to simulate all three experiments with chemical accuracy on the basis of one DF. A problem we address in this connection is that the experiments have not always been described in as much detail as theorists would like; for instance, the parameters characterizing the velocity distributions and rovibrational state distributions of the incident D_2 are often poorly known. To address this, we will simulate all three sticking experiments using four different sets of molecular beam parameters. We also use the time-dependent wave packet (TDWP) method [25, 32] to compute diffraction probabilities on the basis of the SRP−DF, and compare these with the measured values for in-plane and out-of-plane diffraction of Nieto

et al. [21]. Here, the question addressed is whether the SRP−DF previously derived, on the basis of sticking probabilities and based on GGA exchange and van der Waals (non-local) correlation, allows the accurate modeling of diffraction of H_2 from a metal surface.

This chapter is set up as follows. Section 6.2.1 gives an in-depth description of the three sets of supersonic molecular beam experiments that have been performed on sticking of D_2 on Pt(111). Section 6.2.2 discussed the four sets of molecular beam parameters that we have used to simulate these experiments. Section 6.2.3 compares the outcome of the experiments, and discusses which set of molecular beam parameters should in principle be best for simulating each experiment. Section 6.3 discusses the methods we have used. Section 6.3.1 discusses the dynamical model used, Section 6.3.2 the potential energy surface based on the SRP−DF, Section 6.3.3 the dynamics methods employed, Section 6.3.4 the computation of the observables, and Section 6.3.5 provides computational details. Section 6.4 contains the results and discussion, with Section 6.4.1 addressing the simulation of the sticking measurements, and Section 6.4.2 the results for diffraction of H_2. Finally, conclusions are presented in Section 6.5.

6.2 Experiments and beam parameters used to simulate the experiments

In this section we provide a brief description of the three supersonic molecular beam experiments on D_2 + Pt(111) that have been published in the literature [15–17]. In all three publications, results were reported for normal incidence, which we focus on in the present work. We also give a brief description of the four different sets of molecular beam parameters that we have used to simulate the experiments. We finish with a brief discussion of how well the experiments agree with one another, and of which set of parameters should, in principle, be optimal for simulating the three different published experiments.

6.2.1 Molecular beam experiments on D_2 + Pt(111)

The first experiments reported on D_2 + Pt(111) were published by Luntz *et al.*, and we focus on the sticking probabilities S_0 reported in figure 1 of their paper [15], which were measured at a surface temperature (T_s) of

295 K. The sticking probabilities were measured with the King and Wells technique [33]. The beam energies were varied by both changing the nozzle temperature T_n (temperatures up to 1800 K were used) and by seeding D_2 in H_2 (thereby increasing its speed) or in Ne (decreasing its speed). According to the authors, the beam energies were measured with time-of-flight (TOF) techniques to approximately 2 % accuracy. The energies reported were energies averaged over flux weighted velocity distributions [34]. Luntz *et al.* did not report the actual parameters describing their velocity distributions. Luntz *et al.* also reported sticking probabilities for off-normal incidence, for varying polar incidence angles. They also measured the dependence of S_0 on T_s in the range 100-300 K, and reported that for average incidence energies $\langle E_i \rangle$ of 0.075 eV and 0.23 eV S_0 shows only a very small increase with T_s [15].

Subsequently, sticking probabilities of D_2 on Pt(111) were published by Hodgson and co-workers, in the framework of a study on dissociation of D_2 on Sn/Pt(111) surface alloys. The sticking probabilities were reported in figure 5a of their paper, and were measured for a surface temperature of 150 K [16]. Sticking probabilities were measured using temperature programmed desorption measurements calibrated against King and Wells measurements at high incidence energies, and/or using King and Wells measurements directly [35]. The experiments used pure D_2 beams, varying T_n up to a temperature of 2100 K. The experimentalists reported [16] that translational energy distributions were measured with TOF techniques, and that the mean translational energies were related to T_n through $\langle E_i \rangle = 2.75\ k_B T_n$, referring to Ref. [36] for the details of the expansion conditions used. In a private communication [35] Hodgson reported that the incidence energy (E) distributions could be described approximately by exponentially modified Gaussian distributions

$$G(E) = \sqrt{2\pi\sigma}\exp(\frac{-(E - \langle E \rangle)^2}{2\sigma}), \tag{6.1}$$

with σ defined as

$$\sigma = 5.11e^{-3}\langle E \rangle + 1.3184e^{-4}. \tag{6.2}$$

With these definitions, the average incidence energy $\langle E_i \rangle$ is simply equal to $\langle E \rangle$.

Finally, sticking probabilities of D_2 on Pt(111) were published by Cao *et al.* [17], in the framework of a comparison to previously published S_0

computed on the basis of SRP−DFT [9]. We focus on the sticking probabilities S_0 reported in figure 1 of their paper [17], which were measured at $T_s = 200$ K. The sticking probabilities were measured with the King and Wells technique [33]. The beam energies were varied by both changing T_n (temperatures up to 1503 K were used) and by seeding D_2 in H_2 or in Ne, N_2, or Ar. In addition to measuring T_n, the authors conducted TOF experiments to determine the stream velocities v_s and velocity widths α, and taken together with T_n these parameters fully characterize the molecular beams employed. The parameters v_s and α together determine the flux weighted velocity distribution

$$f(v_i; T_n)dv_i = Cv_i^3 e^{-(v_i - v_s)^2/\alpha^2} dv_i, \tag{6.3}$$

and average incidence energies $\langle E_i \rangle$ can be determined by averaging incidence energy over this distribution of incident velocities. The parameters used in the experiments are reported in table 6.1. Cao *et al.* also reported sticking probabilities for off-normal incidence, for varying polar incidence angles and for two planes of incidence.

6.2.2 Sets of molecular beam parameters and their use in simulating molecular beam experiments

In this chapter, we have used four sets of molecular beam parameters to simulate molecular beam experiments. The first set is derived from experiments on D_2 + Ru(0001) [37]. In these experiments, measurements were taken on sticking using pure D_2 beams for five different values of T_n (300, 500, 900, 1300, and 1700 K) , and for D_2 beams seeded in H_2 with two different mixing ratios for T_n = 1700 K. The values of v_s, α, and T_n, which are available from Ref. [38], have been reported in table 3 of Ref. [13]. With the aid of these parameters, sticking probabilities can be computed by velocity averaging (mono-energetic) Boltzmann averaged reaction probabilities $R_{mono}(E_i; T_n)$ over the velocity distribution specified in Equation 6.3 according to

$$R_{beam}(\overline{E}; T_n) = \frac{\int_0^\infty f(v_i; T_n) R_{mono}(E_i; T_n) dv_i}{\int_0^\infty f(v_i; T_n) dv_i}, \tag{6.4}$$

with the incidence energy E_i simply given by the product of half the mass of D_2 with v_i^2 , where v_i is the incident velocity. In turn, the Boltzmann

averaged reaction probability can be computed from the initial (ν, j) state selected reaction probability $P_{deg}(E_i, \nu, j)$ according to

$$R_{mono}(E_i; T_n) = \sum_{\nu,j} F_B(\nu, j; T_n) P_{deg}(E_i, \nu, j). \tag{6.5}$$

with

$$F_B(\nu, j; T_n) = \frac{F(\nu, j; T_n)}{\sum_{\nu,j} F(\nu, j; T_n)}, \tag{6.6}$$

and

$$F(\nu, j; T_n) = (2j+1) e^{\frac{-E_{vib}(\nu)}{k_B T_{vib}}} w(j) e^{-\frac{E_{rot}(j)}{(k_B T_{rot})}}. \tag{6.7}$$

Here, ν is the vibrational, and j the rotational quantum number of D_2, and $w(j)$ is 2 for even j and 1 for odd j. For the rotational temperature, typically $T_{rot} = 0.8\ T_n$ is assumed [39, 40], based mostly on experiments by Gallagher and Fenn [41], and this is what we used to simulate the experiments of Luntz *et al.* [15] and of Cao *et al.* [17]. The assumption made by Hodgson and co-workers that $\langle E_i \rangle = 2.75\ k_B T_n$ corresponds to $T_{rot} = 0.75\ T_n$ and this was used to simulate their experiments [16]. The beam parameters of Groot *et al.* describe molecular beams that are comparatively broad in energy (with large α parameters), as can be seen from figure 1 of Ref. [37].

The second set of parameters describes the beams that were actually used in the D_2 + Pt(111) experiments of Cao *et al.* [17]. As noted above, the values of v_s, α, and T_n are presented in table 6.1. They can be used with Equations 6.3–6.7 to compute sticking probabilities for $\langle E_i \rangle$ in the range 0.10–0.55 eV, with the results corresponding to T_n in the range 490–1520 K. As these parameters describe experiments from the same group as the first set of parameters discussed above, they likewise describe molecular beams that are comparatively broad in energy. The third set of parameters are a set of $\langle E \rangle$, σ, and T_n describing a set of experiments of Hodgson and co-workers on D_2 + Ag(111) [36] for which the expansion conditions were similar to the conditions prevalent in the experiments on D_2 + Pt(111) of the same group [16]. The parameters, which were collected in table 1 of Ref. [42] (see also table 4.1), can be used together with Equations 6.1, 6.2, 6.5–6.7 and

$$R_{beam}(\overline{E}; T_n) = \frac{\int_0^\infty G(E_i; T_n) R_{mono}(E_i; T_n) dE_i}{\int_0^\infty G(E_i; T_n) dE_i}. \tag{6.8}$$

Table 6.1: Parameters used for the molecular beam simulations of D_2 on Pt(111). These parameters are derived from the D_2 + Pt(111) experiments of Cao *et al.* [17].

$\langle E_i \rangle$(eV)	v_s(m/s)	α(m/s)	T_{nozzle}(K)
0.104	2004.6	528.7	473
0.101	2127.9	297.9	673
0.145	2256.8	741.8	673
0.183	2484.9	881.7	973
0.256	3204.7	766.3	673
0.286	3302.7	906.7	873
0.313	3449.1	955.3	873
0.318	3521.1	909.4	873
0.436	4015.0	1181.0	1223
0.444	4096.5	1151.1	1223
0.549	4039.3	1744.7	1503

to compute sticking probabilities for $\langle E_i \rangle$ in the range 0.22−0.49 eV, with the results corresponding to T_n in the range 970−2012 K. For similar $\langle E_i \rangle$ the parameters describe distributions that are symmetric in incidence energy, and beams that are narrower in incidence energy than the beams described by parameter sets 1 and 2 (see figure 2 of Ref. [42], comparing to figure 1 of Ref. [37]).

The fourth set of parameters are once again a set of values of v_s, α, and T_n. They describe molecular beams of a width comparable to the D_2 beams of Hodgson and co-workers, but which do not suffer from the unphysical symmetry in incidence energy [43] present in parameter set 3, as discussed in Ref. [42]. The parameters were obtained from Ref. [44] and describe pure D_2 beam experiments on D_2 + Cu(111) [45], and are collected in table 6.2. (A subset of these parameters were presented in table S9 of Ref. [7]). The parameters can be used to simulate experiments with E_i in the range 0.21-0.45 eV, with the results corresponding to T_n in the range 875-1975 K.

Table 6.2: Parameters used for the molecular beam simulations of D_2 on Pt(111). These parameters are derived from the pure D_2 beam experiments on D_2 + Cu(111) of Auerbach and co-workers [44].

$\langle E_i \rangle$(eV)	v_s(m/s)	α(m/s)	T_{nozzle}(K)
0.207	3134.0	203.0	875
0.244	3392.0	278.0	1030
0.265	3553.0	218.0	1120
0.305	3805.0	259.0	1290
0.340	4014.0	299.0	1435
0.392	4196.0	614.0	1790
0.400	4337.0	371.0	1670
0.430	4374.0	685.0	1905
0.446	4461.0	687.0	1975

6.2.3 Comparison of the measured S_0

The three sets of measured S_0 are shown as a function of $\langle E_i \rangle$ and compared with one another in Figure 6.1. The S_0 of Luntz *et al.* [15] and of Cao *et al.* [17] are in quite good agreement with one another for $\langle E_i \rangle$ up to about 0.32 eV, but for higher $\langle E_i \rangle$ the S_0 measured by Luntz *et al.* [15] are larger. The S_0 of Hodgson and co-workers [16] are smaller than the S_0 measured by Luntz *et al.* [15] and by Cao *et al.* [17] for almost all $\langle E_i \rangle$, except for $\langle E_i \rangle > 0.4$ eV where they exceed the values measured by Cao *et al.*.

To be able to provide a more detailed comparison, we compare the experiments on a one-to-one basis in Figure 6.2. Figure 6.2 (a) shows again that the S_0 of Luntz *et al.* [15] are larger than those of Hodgson and co-workers [16] over the entire energy range. About the origin of this difference we can only speculate. Some of the difference could be due to the lower T_s value used by Hodgson and co-workers (150 K [16] vs. 295 K in the experiment of Luntz *et al.* [15]). Figure 6.1 also shows two results of Luntz *et al.* measured at or interpolated to $T_s = 150$ K (see figure 2 of their paper [15]). The plotted data suggests that at least some of the difference could be due to the lower T_s of Hodgson and co-workers, but is not clear to us how accurately the dependence on T_s was measured by Luntz *et al.*, and

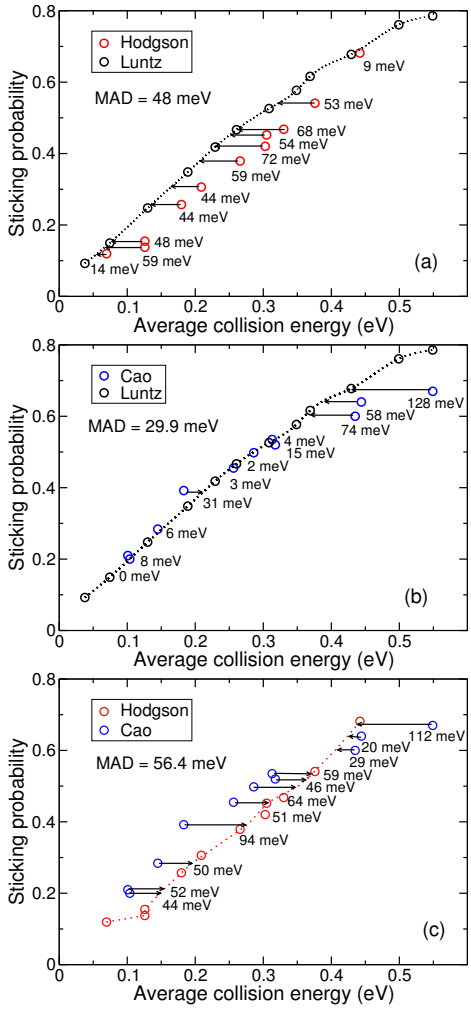

Figure 6.2: A one-to-one comparison of the experiments: (a) comparison of experimental data from Hodgson and co-workers [16] with experimental data from Luntz *et al.* [15], (b) comparison of experimental data from Cao *et al.* [17] with experimental data from Luntz *et al.* [15], and (c) comparison of experimental data from Hodgson and co-workers [16] with experimental data from Cao *et al.* [17]. In the all cases the horizontal arrows and the numbers indicate the energy spacings between the interpolated values of one experiment and the actual values of the other experiment. The dotted lines show the interpolated curve of one set of experimental data.

the T_s dependence of their data for $\langle E_i \rangle = 0.23$ eV would seem rather large for weakly activated dissociation, also in view of the large mass mismatch between D_2 and Pt. We also note that the good agreement between the data of Luntz *et al.* ($T_s = 293$ K) and the data of Cao *et al.* ($T_s = 200$ K, see Figure 6.2 (b)) suggests a weak T_s dependence of sticking between $T_s = 200$ K and 293 K. It is also possible that the difference is due to a calibration problem in the experiments of Hodgson and co-workers, who in some of the measurements used thermal desorption of D_2 to measure S_0, and had to calibrate their measurement on a King and Wells measurement at high $\langle E_i \rangle$. It also seems possible that at least some of the differences are due to the use of seeding gasses in the experiments of Luntz *et al.* [15], whereas Hodgson and co-workers used pure D_2 beams [16]. Specifically, it is possible that T_n was higher in several experiments performed at similar $\langle E_i \rangle$ by Luntz *et al.*, due to the use of a seeding gas that would slow H_2 down.

One way to quantify the discrepancy between the experiments (or between an experimental and a theoretical dataset) is to compute the mean average deviation (MAD) in the average incidence energy at which particular values of S_0 are achieved. This deviation has to be calculated between actual measured (or calculated) values in one experiment, and interpolated values in the other experiment (or calculation). The MAD between the data of Luntz *et al.* [15] and of Hodgson and co-workers [16] is 48 meV, which is larger than 1 kcal/mol (≈ 43 meV). Using 1 kcal/mol as a measure of chemical accuracy, we can then say that the two datasets do not agree to within chemical accuracy.

The datasets of Luntz *et al.* [15] and of Cao *et al.* [17] agree much better with one another (MAD = 29.9 meV, chemical accuracy, see Figure 6.2 (b)), at least for $\langle E_i \rangle$ up to 0.32 eV. This is not true for the larger $\langle E_i \rangle$, where the S_0 of Cao *et al.* are much smaller than those of Luntz *et al.*. It is not clear what this difference is due to. It is likely that for the highest $\langle E_i \rangle$ H_2 was used as a seeding gas in both experiments. At these high incidence energies, the measurement of the beam parameters (and thereby the determination of the $\langle E_i \rangle$) becomes difficult, and it is possible that the E_i was overestimated by Cao *et al.*, or was underestimated by Luntz *et al.*. Another common pitfall with the measurement of a high value of S_0 with the King and Wells method is that the measurement is taken over a time interval where the surface is already partly covered. This could also result in an underestimation of S_0 and could be taken as another indication that

perhaps the S_0 of Cao *et al.* are underestimated as a function of $\langle E_i \rangle$ at $\langle E_i \rangle > 0.4$ eV.

The agreement between the datasets of Cao *et al.* [17] and of Hodgson and co-workers [16] is worst (MAD = 56.4 meV, Figure 6.2 (c)). At the highest values of $\langle E_i \rangle$, the discrepancies can be understood at least in part from the higher T_n values that had to be employed in the pure D_2 beam experiments of Hodgson and co-workers to achieve high $\langle E_i \rangle$ values. However, this is not true for intermediate E_i values, where the S_0 of Cao *et al.* are higher than those of Hodgson and co-workers, even though the T_n values were lower in the experiments of Cao *et al.* [17] (see Figure 6.1). This, and the good agreement between the datasets of Luntz *et al.* [15] and Cao *et al.* for incidence energies up to 0.32 eV would seem to suggest that the measured S_0 of Hodgson and co-workers are too low at least for the lower E_i range.

This also brings us to the question of which set of beam parameters can best be used to simulate the molecular beam experiments. The answer seems obvious for the experiments of Cao *et al.* [17]: for this, the best set of parameters should in principle be the set measured by them [46]. The answer is also fairly straightforward for the experiments of Hodgson and co-workers [16]: for this, the best choice should be the set of parameters available [35] from experiments on D_2 + Ag(111) [36], as they indicated [16] that the expansion conditions in these experiments were the same as in the D_2 + Pt(111) experiments. Also, an alternative would be to use beam parameters from the pure D_2 beam experiments on D_2 + Cu(111) [44, 45], which describe beams with a similar width in incidence energy that possess the appropriate asymmetry with respect to incidence energy [42]. The answer is least obvious for the experiments of Luntz *et al.* [15]. However, the similarity of their results to those of Cao *et al.* [17] suggest that their molecular beam parameters [46] may well be best, with the beam parameters of Groot *et al.* [37] (see Ref. [13]) representing a good alternative, as these experiments [37] come from the same group as those of Cao *et al.*. However, below we will perform simulations using all four sets of beam parameters to describe each of the three experiments, and determine which set leads to the lowest MAD of theory with experiment. Here, it should be noted that the SRP−DF determined for H_2 + Pt(111) was fitted to the experiments of Luntz *et al.* [15], using the beam parameters [13] describing the experiments of Groot *et al.* on D_2 + Ru(0001) [37].

6.3 Method

6.3.1 Dynamical model

The Born-Oppenheimer Static Surface (BOSS) [7] model is used in this study, implying two approximations. First the Born-Oppenheimer (BO) approximation is made, in which the electronic motions are separated from the massive nuclei motions and the ground state potential energy surface (PES) is calculated. In this approximation, electron-hole pair excitation does not affect the reactivity. Second the static surface approximation is made, in which the frozen surface atoms occupy 0 K lattice configuration positions in the (111) surface of the face centered cubic (fcc) structure of the metal. Consideration of these approximations leads to taking 6 molecular degrees of freedom into account in the PES and dynamics calculations. Figure 6.3 (a) shows the coordinate system and Figure 6.3 (b) shows the surface unit cell for the Pt(111) surface and the symmetric sites. With our model we cannot obtain information on the surface temperature dependence of sticking or diffraction.

6.3.2 Potential energy surface

The DFT electronic structure method is used to map out the PES. To compute the PES, the SRP−DF was devised, with the combination of the PBEα [47] exchange functional with the adjustable parameter α and the van der Waals DF2 correlation functional of Langreth and Lundqvist and co-workers [48] as :

$$E_{XC}^{SRP-DF} = E_X^{PBE\alpha} + E_C^{vdW-DF2}$$

where $\alpha = 0.57$ [9]. In total, 29 different molecular configurations distributed over 6 different sites on the surface unit cell shown in Figure 6.3(b) were used to compute and to interpolate the 6D PES. The accurate corrugation reducing procedure (CRP) [49] method was used to interpolate the DFT data calculated on the grid. For more detailed information about the construction of the PES and the interpolation method the reader is referred to Ref. [9].

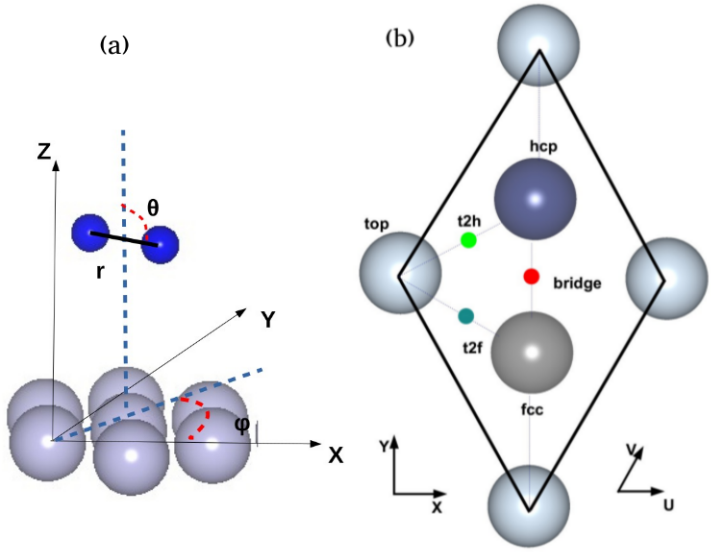

Figure 6.3: (a) The coordinate system for dissociation of H_2 on the Pt(111) surface. In the plot, X, Y, Z are the center of mass coordinates of H_2, r is the H–H distance, and (θ, ϕ) are the polar and azimuthal angles specifying the orientation of the H–H bond with respect to the surface. (b) The schematic picture of the surface unit cell is indicated by a diamond shaped line connecting four top sites. The sites considered which are used for CRP interpolation, larger solid circles show the surface atoms and the small colored solid circles show the high symmetry sites. Two choices of coordinate system are indicated, a skewed coordinate system (U, V) and a Cartesian coordinate system (X, Y). Light blue atoms are in the top layer, dark blue atoms are in the second layer, and gray atoms are in the third layer.

6.3.3 Dynamics methods

To compute dissociation probabilities for D_2 impinging on the Pt(111) surface the QCT method [50] was used. In this method the initial zero-point-energy (ZPE) of the molecule is taken into account, and the initial conditions are chosen with Monte Carlo sampling. The selection of the ori-

entation of the molecule, θ, and ϕ, is based on the selection of the initial rotational state. We used the fixed magnitude of the classical initial angular momentum according to $L = \sqrt{j(j+1)}/\hbar$, and its orientation, while constrained by $\cos\Theta_L = m_j/\sqrt{j(j+1)}$, is otherwise randomly chosen as described in [13, 51]. Here, j is the rotational quantum number, m_j is the magnetic rotational quantum number and Θ_L is the angle between the angular momentum vector and the surface normal. The impact sites are chosen at random.

The TDWP method was used to compute diffraction probabilities for H_2 scattering from Pt(111). This method is fully described in Ref. [25] (see also Section 2.5.2).

6.3.4 Computation of the observables

Initial state resolved reaction probabilities

Initial state resolved reaction probabilities $P_{deg}(E;\nu,j)$ are obtained by degeneracy averaging the fully initial state resolved reaction probabilities $P_r(E;\nu,j,m_j)$ according to

$$P_{deg}(E;\nu,j) = \frac{\sum_{m_j=0}^{m_j=j}(2-\delta_{m_j0}).P_r(E;\nu,j,m_j)}{(2j+1)} \tag{6.9}$$

where P_r is the fully initial state–resolved reaction probability, and δ is the Kronecker delta. Sections 6.2.1 and 6.2.2 have described how the degeneracy averaged sticking probabilities can be used to compute sticking probabilities for comparison with molecular beam experiments.

Diffraction probabilities

To study diffraction, a quantum phenomenon, quantum dynamics calculations should be performed as was done before for H_2 + Pt(111) [25]. In the diffractive scattering process, the molecules translational momentum parallel to the surface can only change by discrete amounts. In order to compare with the experimental diffraction probabilities [21], the rovibra-

tionally elastic diffraction probabilities are computed by

$$P_{nm}(E;\nu,j,m_j) = \sum_{m_j^{'}=-j}^{j} P_{scat}(E;\nu,j,m_j \rightarrow \nu' = \nu, j' = j, m_j^{'}, n, m), \tag{6.10}$$

where P_{nm} is the rovibrationally elastic probability for scattering into the diffraction state denoted by the n and m quantum numbers. These probabilities are degeneracy averaged by

$$P_{nm}(E;\nu,j) = \sum_{m_j=-j}^{j} P_{nm}(E;\nu,j,m_j)/(2j+1). \tag{6.11}$$

The reciprocal lattice corresponding to the direct lattice is shown in Figure 6.4. The diffraction order O_d is also shown here. In the definition we use [21], the N^{th} diffraction order consists of all diffraction channels on the N^{th} concentric hexagon. The first order diffraction channels (1, 0), (−1, 0), (0, 1), (0, −1), (1, 1) and (−1, −1) correspond to a momentum change of one quantum Δk. We obtained probabilities for scattering of cold n-H_2 (20% $j = 0$, 75% $j = 1$, 5% $j = 2$) [52] scattering from Pt(111) with an initial translational energy parallel to the surface of 0.055 eV.

6.3.5 Computational details

For the electronic structure calculations VASP (version 5.2.12) was used [53–56]. A plane wave basis set was used for the electronic orbitals and the XC functional used has been described and discussed in Section 6.3.2. Furthermore the standard PAW pseudopotentials [57] were used for the ion cores, and we used the scheme of Román-Pérez and Soler [58] to evaluate the vdW-DF2 correlation energy. Further details on the computation and interpolation of the PES have been provided in [9].

At least 10000 trajectories were computed in the QCT calculations for each initial set (E_i, ν_i and j_i), sampled equally over the possible initial m_j states. In the calculation of the sticking probability and the Boltzmann averaging (Equation 6.5), the maximum vibrational quantum number was 3 and the maximum rotational quantum number was 20. The center of mass of the D_2 molecule was initially placed at $Z = 9$ Å. If the D−D distance becomes larger than 2.25 Å the D_2 molecule is considered to be dissociated.

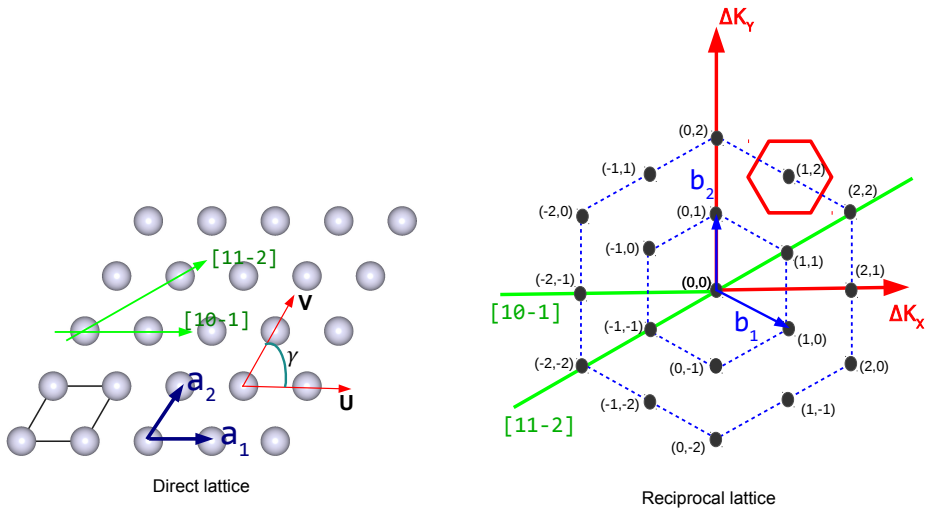

Figure 6.4: The direct (the left plot) and the reciprocal lattice (the right plot) for an fcc(111) surface. In the direct lattice γ is the skewing angle, and a_1 and a_2 are the primitive vectors that span the surface unit cell. Miller indices are shown in the reciprocal lattice to indicate the different diffraction channels. Red hexagon shows the 2D Wigner–Seitz cell. The concentric hexagons indicate how the diffraction order is defined for the (111) lattice. The $\langle 10\bar{1} \rangle$ and $\langle 11\bar{2} \rangle$ directions have been indicated in both figures in green.

Otherwise the D_2 molecule is considered to be reflected from the surface to the gas phase when its distance to the surface in Z exceeds 4.0 Å and D_2 has a velocity towards the vacuum. The reaction probability was calculated as the ratio of the number of dissociated trajectories and the total number of trajectories run.

Table 6.3 lists the relevant parameters used in the 6D QD calculations for the scattering of ($\nu = 0$, $j = 0$) H_2. To cover the collision energy range $E = 0.05 - 0.55$ eV, two wave packet calculations were performed for two separate energy ranges: 0.05 to 0.20 eV and 0.15 to 0.55 eV. This procedure

Table 6.3: Input parameters for the quantum dynamical calculations on H_2 dissociating on Pt(111) in the energy range of [0.05−0.20]eV. All values are given in atomic units. The abbreviation "sp" refers to the specular grid used to bring in the initial wave function.

Parameter	**Description**	**Value**
$N_X = N_Y$	no. of grid points in X and Y	16
N_Z	no. of grid points in Z	256
$N_{Z(sp)}$	no. of specular grid points	256
ΔZ	spacing of Z grid points	0.135
Z_{min}	minimum value of Z	-1.0
N_r	no. of grid points in r	40
Δr	spacing of r grid points	0.2
r_{min}	minimum value of r	0.4
j_{max}	maximum j value in basis set	24
m_{jmax}	maximum m_j value in basis set	16
Δt	time step	5
T_{tot}	total propagation time	82000
Z_0	center of initial wave packet	16.955
Z_{inf}	location of analysis line	12.5
Z^{opt}_{start}	start of optical potential in Z	12.5
Z^{opt}_{end}	end of optical potential in Z	33.425
A_Z	optical potential strength in Z	0.00072
r^{opt}_{start}	start of optical potential in r	4.2
r^{opt}_{end}	end of optical potential in r	8.2
A_r	optical potential strength in r	0.0096
$Z(sp)^{opt}_{start}$	start of optical potential in $Z(sp)$	22.355
$Z(sp)^{opt}_{end}$	end of optical potential in $Z(sp)$	33.425
$A_{Z(sp)}$	optical potential strength in $Z(sp)$	0.0035

avoids problems which may arise from the interaction of the optical potential with the low translational energy components of the wave packet, if only one broad Gaussian initial wave packet is used to cover the entire range.

6.4 Results and discussion

6.4.1 Sticking probabilities

To simulate the molecular beam sticking probabilities four different sets of molecular beam parameters are available. To distinguish these sets of parameters, here we introduce acronyms. As discussed in Section 6.2.2, the first set of parameters was extracted from experiments on D_2 + Ru(0001) [37], and we call this parameter set SBG, where S stands for seeded beams, B for broad in translational energy, and G for Groot *et al.* [37]. The second set of parameters is derived from the D_2 + Pt(111) experiments of Cao *et al.* [17], and we call this parameter set SBC. The third set of parameters (PNH) was reported in Ref. [42] to describe experiments of Hodgson and co-workers on D_2 + Ag(111) [16], and in this acronym P stand for pure D_2 beam, N for narrow, and H for Hodgson and co-workers. The last set of parameters (PNA) describe pure D_2 beam experiments on D_2 + Cu(111) using translationally narrow beams [44].

Figure 6.5 shows a comparison of the theoretical sticking probabilities for the four sets of parameters. The match between all sets of theoretical results is quite good for $\langle E_i \rangle$ up to 0.32 eV. Based on the theory, we would then expect that there should be excellent agreement between the experiments of Cao *et al.* [17] (described by the parameter set SBC) and Hodgson and co-workers (parameter sets PNH and PNA) at $\langle E_i \rangle$ up to 0.32 eV. However, the agreement between the S_0 measured by these two groups is rather poor (see Figure 6.1 and Figure 6.2 (c)). Given that the two parameter sets SBC and PNH represent two extremes (of seeded beams that are broad in translational energy and pure beams that are narrow in energy), we should also expect good agreement of both of the experiments referred to above with the S_0 measured by Luntz *et al.* [15], for which no beam parameters are available. The good agreement obtained of these S_0 with the measurements of Cao *et al.* (Figure 6.1 and Figure 6.2 (b)), and the poor agreement with the measurements of Hodgson and co-workers for $\langle E_i \rangle \leq 0.32$ eV then suggests that for some reason the S_0 measured by Hodgson and co-workers were too small.

A difference in the theoretical S_0 appears at $\langle E_i \rangle > 0.32$ eV between the results obtained with pure and narrow beams on the one hand, and with seeded and broad beams on the other hand (Figure 6.5). The S_0 computed with the parameter sets PNH and PNA exceed those computed with the

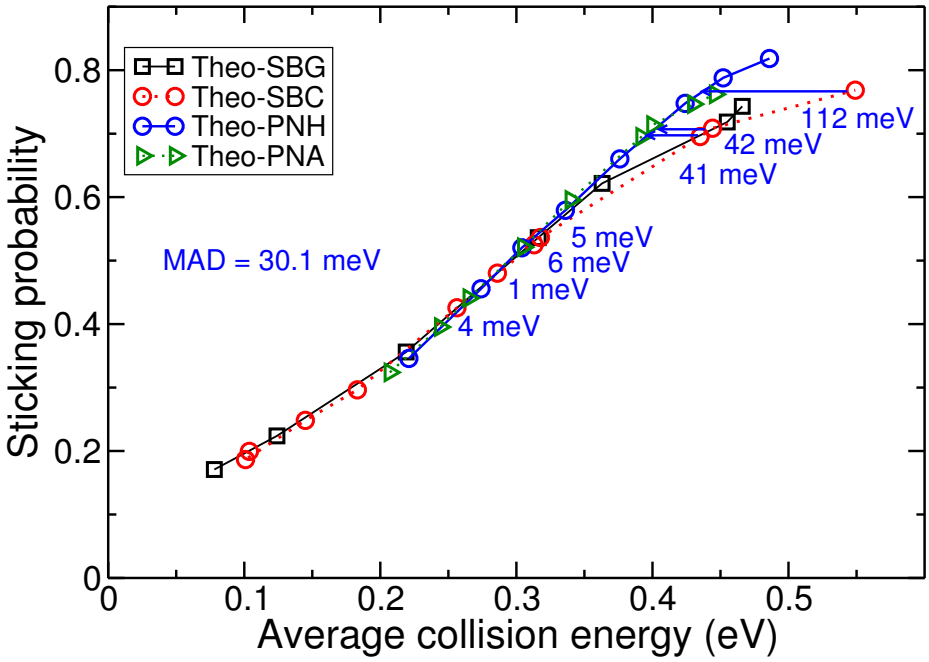

Figure 6.5: Comparison of sticking probabilities computed with different sets of parameters. Black symbols show the theoretical results obtained with the SBG parameters, red symbols the theoretical results with SBC. Blue and green symbols show the computed results obtained with the PNH and PNA parameters, respectively. The arrows and the numbers show the energy differences between the results obtained with the SBC parameters and interpolated values of the results obtained with the PNH parameters.

parameter sets SBG and SBC for higher energies. To understand the reason of the observed effect, we tested the effects of averaging the reaction probability over the translational energy distributions and over the rovibrational states separately. Boltzmann averaging the reaction probability based on nozzle temperature to obtain $R_{mono}(E_i; T_n)$ similarly increases the reaction probability for the pure and for the seeded beams (see Figure 6.A.1 of the Appendix).

However, averaging over the translational energy decreases the reaction probability more for the broader energy distributions used in the seeded beam experiments than for the narrow energy distributions used in the

Table 6.4: MAD values in (eV) characterizing the agreement between three different sets of experimental results and the theoretical results obtained with four different sets of molecular beam parameters.

	Exps	**Luntz**	**Hodgson**	**Cao**
parameters				
SBG		13.5	34.6	37.4
SBC		13.3	35.6	36.9
PNH		35.1	45.0	54.0
PNA		26.1	47.0	54.5

pure D_2 experiments (Figure 6.A.1). The reason for this is twofold: (i) at higher incidence energies E_i and for the weakly activated dissociative chemisorption problem under consideration, the slope of the reaction probability as a function of E_i becomes a decreasing function of E_i, and (ii) most molecules collide with the surface with $E_i \leq \langle E_i \rangle$. Therefore, averaging over the translational energy distribution decreases the measured S_0, and it does so more for translationally broader beams. Looking at the actual experimental results (Figure 6.1 and Figure 6.2 (a), and Figure 6.2 (c)) we see that the predicted trend is observed, although the $\langle E_i \rangle$ at which the pure, narrow beam experiments yield higher S_0 than in the seeded, broad beam experiments is shifted to higher energies, again suggesting that the S_0 measured by Hodgson and co-workers are too small.

Figure 6.6 shows a comparison of the experimental data reported by Luntz *et al.* [15], for which no beam parameters were reported, and the results of our simulations with the SBG parameters. The sticking probabilities of Luntz *et al.* [15] are quite well described with this parameter set (well within chemical accuracy, MAD = 13.5 meV, see table 6.4). This experiment is also quite well described with the SBC set (MAD = 13.3 meV, see Figure 6.A.2 (a) and table 6.4).

The experimental data are also reproduced reasonably well with the parameter sets describing narrower beams (MAD = 26.1 meV for PNA and 35.1 meV for PNH, table 6.4 and Figures 6.A.2 (b) and (c)). However, the larger MADs obtained with the narrower beams suggests that the beams used by Luntz *et al.* were broad in translational energy, similar to the beams employed by Juurlink and co-workers. A caveat is that the SRP−DF was

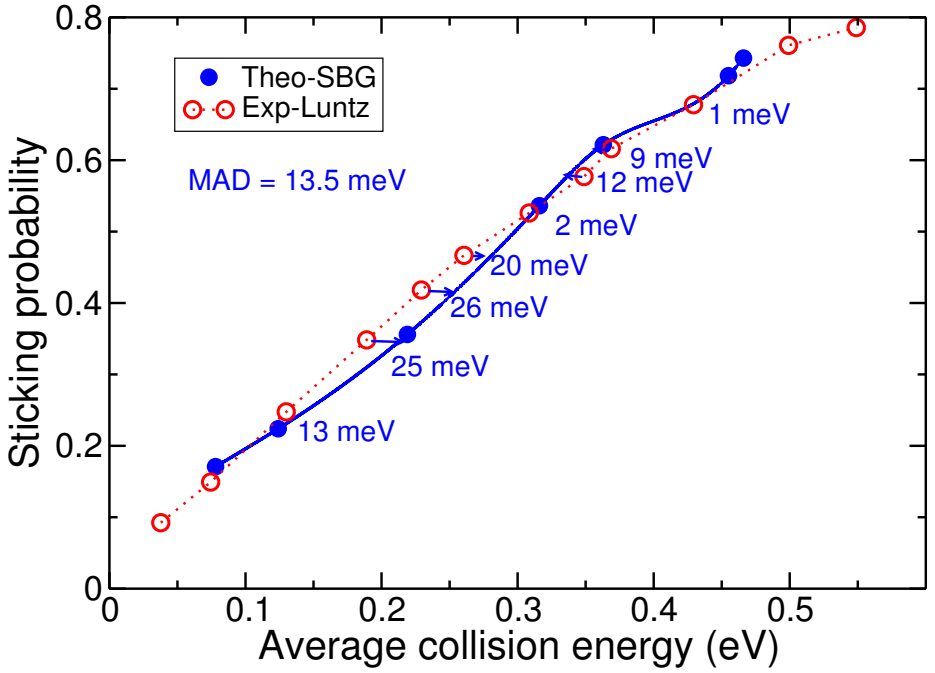

Figure 6.6: Computed sticking probabilities (blue symbols) are shown as a function of $\langle E_i \rangle$ along with the experimental results (red symbols) of Luntz *et al.* [15]. The arrows and accompanying numbers show the energy differences between the experimental data and the interpolated theoretical sticking probability values.

fitted to the experiments of Luntz *et al.* using the SBG set of parameters, and this may affect the conclusion just arrived at, by biasing the SRP functional to yield better results for the broader beams.

The S_0 measured by Hodgson and co-workers [16] are still described to within chemical accuracy with the SBG parameters (Figure 6.7 (a)), albeit that the MAD (34.6 meV) is much higher than obtained for the experiment of Luntz *et al.* (13.5 meV, see table 6.4). A similar conclusion applies for the SBC parameter set (Figure 6.A.3 (a) and table 6.4).

However, with the two other sets of parameters, which should actually describe the beams used in the experiments of Hodgson and co-workers (see Section 6.2), our simulations cannot reproduce these experiments within

chemical accuracy (Figure 6.7 (b) and Figure 6.A.3 (b)). Specifically, MAD values are obtained of 45.0 meV and 47.0 meV for the PNH and PNA sets, respectively. However, if we multiply the measured S_0 with a factor 1.13, excellent agreement (MAD = 12.7 meV) with the theoretical S_0 is obtained using the PNH set (Figure 6.7 (c)). This finding represents additional evidence that the S_0 measured by Hodgson and co-workers were too low, as it is unlikely that the effect is caused entirely by the use of a lower T_s (150 K) than employed by Luntz *et al.* (293 K) and Cao *et al.* (200 K, see Figure 6.1). A possible reason for this could be that at least in some of the experiments thermal desorption was used to measure the amount of adsorbed D_2, with calibration to values of S_0 determined with one or more King and Wells measurements performed for high $\langle E_i \rangle$ (see also Section 6.2). If the King and Wells measurements for some reason returned too low values of S_0, this should affect the subsequent thermal desorption measurements of S_0 in a similar way. Possible reasons for King and Wells measurements returning too low S_0 values include the use of a duty cycle that is too high, or the use of a time-interval in the King and Wells measurement that is too long, so that the sticking probability is determined for an already partially covered surface. These problems may become aggravated and lead to systematic errors if the King and Wells measurement is carried out only for a high $\langle E_i \rangle$ for which S_0 is high, and if the King and Wells measurement is carried out for calibration purposes.

The S_0 measured by Cao *et al.* [17] are best described (and still to within chemical accuracy) with the beam parameter set SBC describing these experiments (MAD = 36.9 meV), Figure 6.8 and table 6.4). Figure 6.A.4 (a) shows similar agreement between the experiments of Cao *et al.* and the theoretical results obtained with the SBG set (MAD = 37.4 meV, table 6.4).

In both cases there are, however, large discrepancies between theory and experiments at the highest $\langle E_i \rangle$. The simulations using parameters describing narrow beams (PNH and PNA) cannot describe the experiments of Cao *et al.* with chemical accuracy (MAD values of 54.0 and 54.5 meV, respectively, see Figures 6.A.4 (b) and (c) and table 6.4). Also, much better descriptions of the experiments of Luntz *et al.* [15] than of the experiments of Cao *et al.* were obtained with the SBG and SBC parameter sets. This could be due to two reasons.

First of all, the SRP−DF has been fitted [9] to the experiments of Luntz *et al.* [15] using the SBG parameter set, and this could bias the SRP−DF to a better description of the experiments of Luntz *et al.*. Second, we suspect

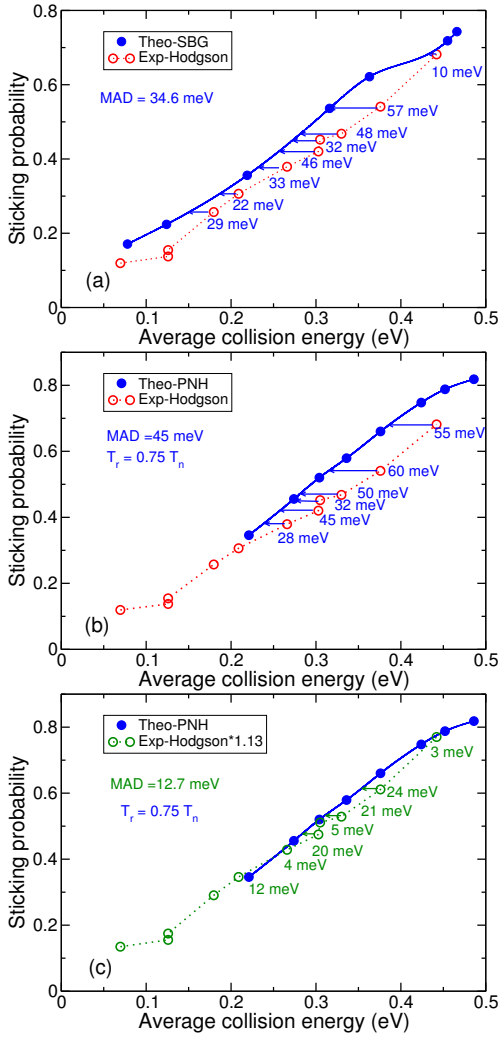

Figure 6.7: Comparison between the molecular beam sticking probabilities for the experiments of Hodgson and co-workers [16] and theoretical results obtained with two sets of parameters: (a) computed data with the SBG set of parameters (b) computed data with the PNH parameters. (c) The last panel shows the comparison between the experimental values of Hodgson and co-workers multiplied with 1.13 and the theoretical results obtained with the PNH set of parameters. The arrows with numbers show the energy spacings between the experimental values and the interpolated theoretical data. The blue curve shows the interpolated theoretical results in all cases.

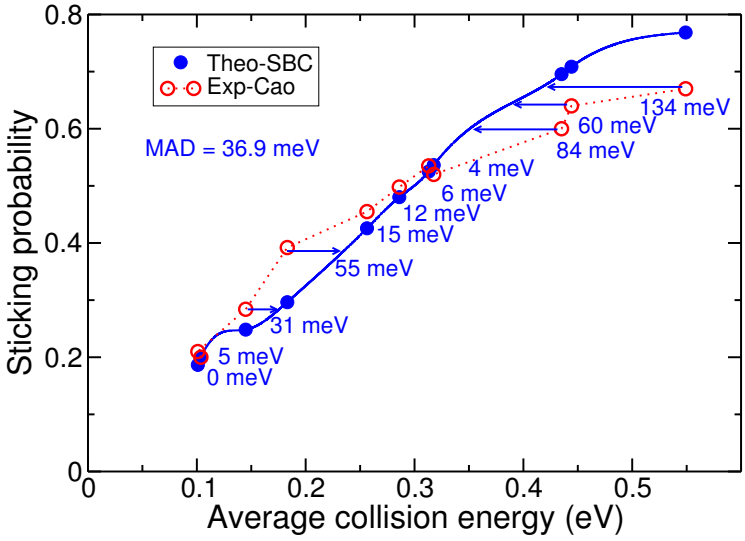

Figure 6.8: Comparison between the molecular beam sticking probabilities for the experiments of Cao *et al.* [17] and the theoretical results obtained with the set of parameters SBC. The arrows and numbers show the energy spacings between the experimental values and the interpolated theoretical data. The blue curve shows the interpolated theoretical results.

that the SBC beam parameters contain errors at the high $\langle E_i \rangle$. The reason for that is that, in recent experiments on H_2 and D_2 + Pt(211) employing pure hydrogen beams, in most cases $\langle E_i \rangle$ exceeded $3k_BT_n$ rather than being approximately $2.7k_BT_n$ [Ref. [59]], as would be expected for pure hydrogen beams [41]). As a result, the incidence energies were likely to be overestimated at high $\langle E_i \rangle$ in these experiments. We suspect that the experiments of Cao *et al.* in figures 2 and 3 of their paper are similarly affected, and as a result for high $\langle E_i \rangle$ the measured S_0 should be underestimated. An explanation [Ref. [59]] is that parameters describing the translational energy distributions of hydrogen beams become progressively harder to determine accurately for higher $\langle E_i \rangle$, due to the corresponding shorter times of flight. An alternative explanation for $\langle E_i \rangle > 2.7\ k_BT_n$ in the experiments is that the actual T_n could have been higher than the measured value. However, this does not explain the sign of the difference between the simulated and measured S_0; if we would underestimate the nozzle temperature in per-

forming the Boltzmann average, we would expect that the theory should underestimate the measured value of S_0 at high $\langle E_i \rangle$ (see Figure 6.A.1), but the opposite is the case (see Figure 6.8). On the other hand, the theory could overestimate the measured reaction probability at high $\langle E_i \rangle$ if for some reason the expansion gas would not be fully equilibrated with the nozzle at the highest T_n, so that the gas temperature would be lower than T_n. It is not clear to us whether this might have been the case in the experiments of Cao *et al.*.

6.4.2 Diffraction probabilities

The comparison of the theoretical results with the absolute diffraction probabilities extracted from the measured angular distributions by Nieto *et al.* [21] is shown in Figures 6.9 (a) and (b), and Figures 6.10 (a) and (b) for the $\langle 1, 0, \bar{1} \rangle$ and $\langle 1, 1, \bar{2} \rangle$ incidence directions, respectively. In these figures the diffraction probabilities are plotted against the total incidence energy for off-normal incidence for the PBEαvdW-DF2 XC functional. Increasing the impact energy increases the number of open diffraction channels and this appears to lead to a substantial drain of flux out of the specular channel in the experiment. However, a similar decrease is not observed in the calculations. Along the $\langle 1, 0, \bar{1} \rangle$ incidence direction, as we can see in Figure 6.9 (b), the most important first order diffraction channel is made up by the two almost equivalent out-of-plane diffraction channels, $(0, -1)$ and $(0, 1)$ (see also Figure 6.4). The energy transfer into these two diffraction channels, *i.e.* $(0, -1)$ and $(0, 1)$, is independent of the initial momentum because the parallel momentum change is perpendicular to the plane of incidence. For the other four diffraction channels, there is a component that is parallel to the incidence plane. Diffractive scattering probabilities for these diffraction channels are smaller because of the larger energy transfer involved [21, 60].

As shown in Figure 6.9, diffraction probability curves for the zero and first order diffraction channels do not show a dramatic change over the considered energy range. A quantitative comparison of the results displays that there is a large discrepancy between theory and experiment for $P0$. However, comparing with experiment, the order of the size of the (sum of the) diffraction probabilities, $P0$ and $[P(0,1) + P(0,-1)]$, is correctly described. In our calculations, the order in the size of $[P(-1,0)+P(-1,-1)]$ and $[P(1,1) + P(1,0)]$ is not correctly described. Looking at $[P(0,1) + P(0,-1)]$, $[P(-1,0) + P(-1,-1)]$ and $[P(1,1) + P(1,0)]$, overall there is a

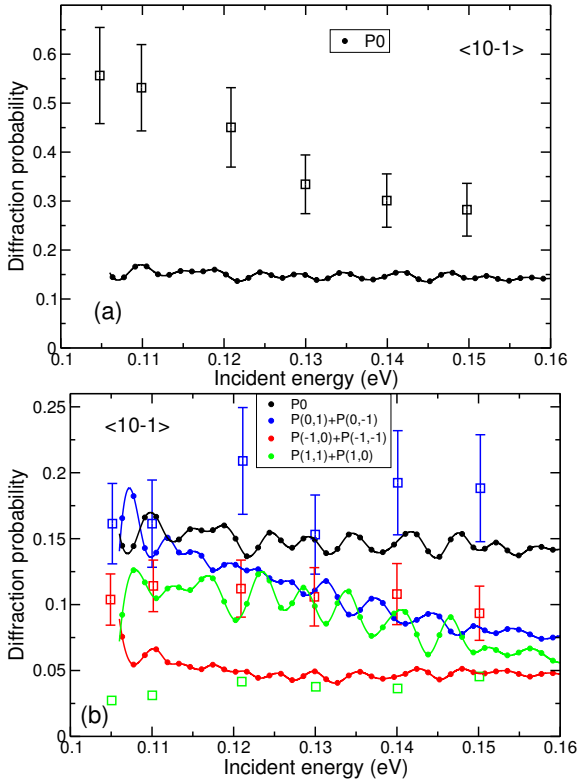

Figure 6.9: Diffraction probabilities for n-H_2 (20 % $j = 0$, 75 % $j = 1$, 5 % $j = 2$) scattering : (a) Specular scattering (black) and (b) several first order out-of-plane diffractive scattering transitions from Pt(111) with an initial parallel energy of 55 meV along the $\langle 1, 0, \bar{1} \rangle$ incidence direction computed with the PBEα-vdW-DF2 XC functional. For comparison, experimental results are shown (symbols with error bars). The probabilities for symmetry equivalent transitions are summed.

rather poor agreement between theory and experiment for these diffraction channels, regardless of the order in the size.

Figure 6.10 shows diffraction probabilities for scattering along the $\langle 1, 1, \bar{2} \rangle$ incidence direction. The probability for specular scattering $P0$ (Figure 6.10 (a)) is larger than the first order in–plane diffraction probabilities $P(1, 1)$, $P(-1, -1)$ (Figure 6.10 (b)), the sum of the first order sideways backward diffraction probabilities $[P(-1, 0) + P(0, -1)]$, and the sum of the first or-

der sideways forward diffraction probabilities $[P(1,0) + P(0,1)]$. The results from the PBEα-vdW-DF2 XC functional underestimate the measured specular scattering probability $P0$. In the experiment, the sums of the first order out-off-plane diffraction channels, $[P(-1,0)+P(0,-1)]$ and $[P(1,0)+P(0,1)]$ show a higher probability than the first order in-plane diffraction channels, $P(1,1)$ and $P(-1,-1)$. The experiment also found smaller probabilities for in-plane and out-off-plane diffraction relative to specular scattering. In the intermediate energy range the sizes of $[P(-1,0) + P(0,-1)]$ and $[P(1,0) + P(0,1)]$ are almost similar in both theory and experiment. Over most of the energy range the computed $P(1,1)$ is larger than the computed $P(-1,-1)$ which is in disagreement with experiment and previous theoretical results [21]. Overall, the quantitative agreement between theory and experiment is rather poor, also for this incidence direction.

The agreement for diffraction compared to experiments is clearly not as good as the agreement obtained for the reaction probabilities. There are both qualitative and quantitative differences. The computed zero order diffraction probabilities are too low compared to the experiments. Another difference between our results and previous theoretical results by Nieto *et al.* [21] is that the older theoretical results, which were based on the B88P86 [29, 30] GGA functional, better reproduced the order in the first order diffraction probabilities [21].

Comparison of diffractive scattering of H_2 from Cu(111) [61] obtained with PESs based on PW91 and RPBE functionals demonstrated that diffraction spectra are much more sensitive to the details of the PES than sticking probabilities. Therefore, the diffraction experimental data are very useful to test the accuracy of the PES and in turn the accuracy of the DFT functional. The present comparison between the theory and the experiment suggests that the SRP−DF for H_2 + Pt(111) may not yet be accurate enough to describe the diffraction in the H_2 + Pt(111) system.

We have previously discussed another potential source of discrepancy between measured diffraction probabilities and diffraction probabilities computed with a PES exhibiting a van der Waals well [13]. It is important to realize that the experimental diffraction probabilities shown in Figures 6.9 and 6.10 were not directly measured for a 0 K Pt(111) surface, and certainly not for a rigid surface, as assumed in the theory. Rather, these data were obtained by performing a DW extrapolation of data measured between 500 and 1000 K [21]. DW theory assumes direct scattering. However, our PES exhibits a van der Waals well of 72 meV, and at the normal incidence range

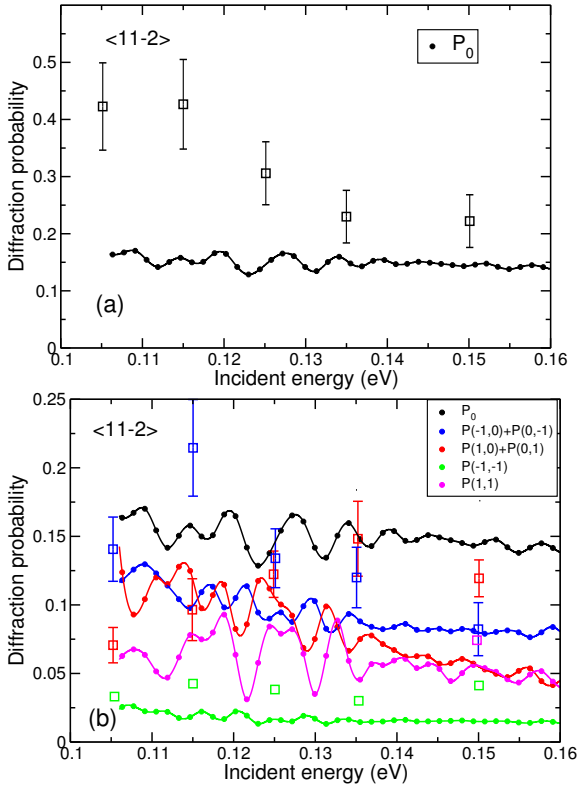

Figure 6.10: Comparison of the experimentally determined diffraction probabilities (symbols) with diffraction probabilities computed with the PBEα-vdW-DF2 XC functional for (a) specular scattering (black) and (b) several first order out-of-plane (blue and red) and in-plane (green and pink) diffractive transitions for incidence along the $\langle 1, 1, \bar{2} \rangle$ incidence direction for n-H_2 (20 % $j = 0$, 75 % $j = 1$, 5 % $j = 2$) from Pt(111) with an initial parallel energy of 55 meV. The probabilities for symmetry equivalent transitions are summed.

of energies addressed here, part of the scattering should be indirect, as also indicated by the oscillatory behavior of the computed diffraction probabilities in Figures 6.9 and 6.10. If we were to take this into account in the DW attenuation, assuming that with each bounce on the surface there is again a probability of phonon excitation, this should lead to decreased "experimental" diffraction probabilities, by amounts that might differ among

the channels. In other words, it is possible that the theory is quite good for the hypothetical case of scattering from a 0 K surface, but that the experimental 0 K result is wrong because standard DW extrapolation to 0 K was not applicable. In this respect, GGA PESs might seem to give good results for diffraction (as observed in Ref. [21]) and for many other H_2-metal systems [62], because it applies to the hypothetical case of scattering from a surface with the van der Waals well discarded, for which DW attenuation should actually work reasonably well. This can be tested by computing diffraction probabilities for scattering from a thermal Pt(111) surface, allowing excitation of the phonons. Alternatively, it might be possible to test the corrugation of the repulsive part of the H_2 + Pt(111) PES by removing the van der Waals well to obtain a purely repulsive PES, and computing diffraction probabilities for this PES [31]. Finally it might be possible to model the attenuating effect of phonon excitation with the aid of an optical potential [63].

In previous work on H_2 + Ru(0001), we found that the agreement between experiment and theory with inclusion of a van der Waals well in the PES could be improved by assuming a specific type of static surface disorder of the metal surface [31]. However, making this assumption will deteriorate rather than improve the agreement between theory and experiment. The reason is that making this assumption will lead to decreased computed diffraction probabilities, and this will worsen the already bad agreement for specular scattering even more.

6.5 Conclusions

This paper tackles two problems faced by the SRP−DFT approach. The first problem is that the SRP−DFT approach is obviously no more accurate than the underlying experimental data are. The second problem is that it is hard to validate a candidate SRP−DF on the basis of a comparison between theoretical and experimental diffraction probabilities for H_2- metal systems.

To address the first problem of the SRP−DFT approach, we have simulated all three sets of measurements of sticking probabilities available for D_2 + Pt(111), using four different sets of molecular beam parameters. As discussed in the paper, substantial differences exist between the three sticking probability curves measured for D_2 + Cu(111). We compared these experiments on a one-to-one basis. The comparison showed that the sticking

probability of Luntz *et al.* [15] are larger than those of Hodgson and co-workers [16] over the entire energy range. The datasets of Luntz *et al.* [15] and of Cao *et al.* [17] showed much better agreement at least for collision energies up to 0.32 eV, but not for larger collision energies. The agreement between the datasets of Cao *et al.* [17] and of Hodgson and co-workers [16] was poorest. We discussed the origin of these discrepancies and reported the MADs between the data of the experiments.

Next we described the four different sets of molecular beam parameters that we have used in our calculations to simulate the experiments. We also discussed the question of which set of beam parameters can best be used to simulate a particular set of molecular beam experiments.

To construct the PES, the CRP interpolation method was used to accurately fit DFT data based on the PBEα-vdW-DF2 functional with $\alpha = 0.57$. This functional was previously found to enable a chemically accurate description of the experiments of Luntz *et al.* [9]. We have performed calculations within the BOSS dynamical model. The QCT method has been used to compute molecular beam sticking probabilities using velocity averaging and Boltzmann averaging for each set of molecular beam parameters. We have shown the comparison of our theoretical results for the four sets of parameters with each other. The agreement between the results obtained with all sets of parameters is quite good for average collision energies up to 0.32 eV.

We have discussed the discrepancy between the theoretical results for translationally narrow and broad beams at the higher collision energies. Comparison between the theoretical results obtained with four sets of parameters and the three sets of experimental data has also been made. MAD values for three different experimental results and four different sets of theoretical results were reported and the success or failure of achieving a chemically accurate description of these three sets of molecular beam experiments was discussed separately. The most important result is that all three sets of experiments can be described with chemical accuracy using molecular beam parameters describing seeded molecular beams that are broad in energy. Performing simulations with different sets of molecular beam parameters also provides insight into under which conditions the experiments should agree with one another. This allows one to arrive at conclusion regarding problems that might affect the experiments. For instance, the simulations suggested that the sticking probabilities measured by Hodgson and co-workers were too low by about 13%, although we cannot rule out

completely that part of this difference might have been due to the use of a lower T_s.

To address the second problem of the SRP−DFT approach, we performed diffractive scattering calculations comparing with experiments, using the SRP−DF. To compute diffraction probabilities for H_2 scattering from Pt(111) the TDWP method was used and probabilities were obtained for scattering of cold n-H_2(20% $j = 0$, 75% $j = 1$, 5% $j = 2$) scattering from Pt(111) with an initial translational energy parallel to the surface of 55 meV. The theoretical results have been shown and compared with experimental results for off-normal incidence for two incidence directions. The agreement for diffraction compared to experiments was rather poor in contrast with the agreement obtained for the sticking probabilities. The results show both quantitative and qualitative discrepancies between theory and experiments. The previous theoretical results by Nieto *et al.* [21], which were based on the use of a GGA functional, demonstrated better agreement with the experiments. Our study suggests that the SRP−DF for H_2 + Pt(111) may not yet be accurate enough to describe the diffraction in this system. Also with the use of a PES exhibiting a van der Waals well, part of the scattering should be indirect. However, the DW theory used to obtain 0 K experimental diffraction probabilities, assumes direct scattering. The previous study has shown that the agreement between experiment and theory with inclusion of a van der Waals well in the PES was improved by assuming a static surface disorder of metal surface for H_2 scattering from Ru(0001) [31]. However, as discussed making this assumption will not improve the agreement between theory and experiment in the case of H_2 scattering from Pt(111).

6.A Appendix

This appendix contains comparison of sticking probabilities for two sets of parameters Figure 6.A.1; comparison of the experimental data from Luntz *et al.*, Hodgson and co-workers, and Cao *et al.* with theortical results (Figure 6.A.2, Figure 6.A.3 and Figure 6.A.1).

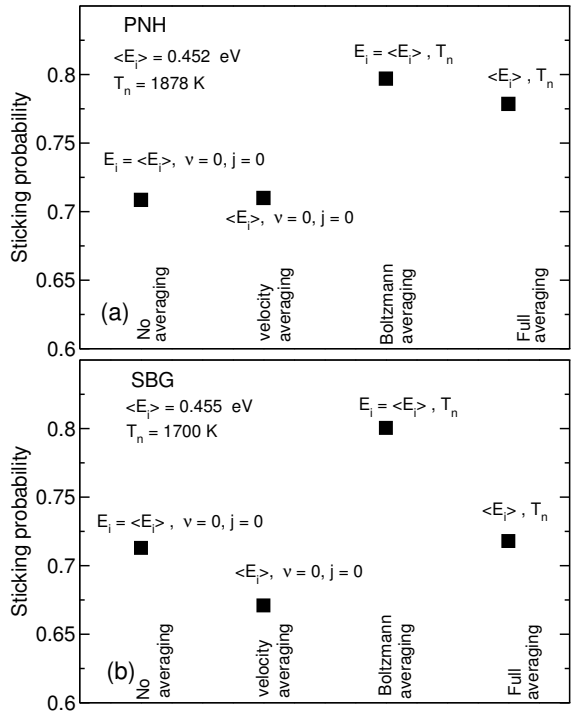

Figure 6.A.1: Comparison of sticking probabilities for two sets of parameters: (a) PNH with narrower energy distributions and (b) SBG with wider energy distributions. Shown are the reaction probability of $(\nu = 0, j = 0)$ D_2 without velocity averaging, the reaction probability of $(\nu = 0, j = 0)$ D_2 with velocity averaging, the reaction probability with Boltzmann averaging over rovibrational states only, and the sticking probability computed with full averaging.

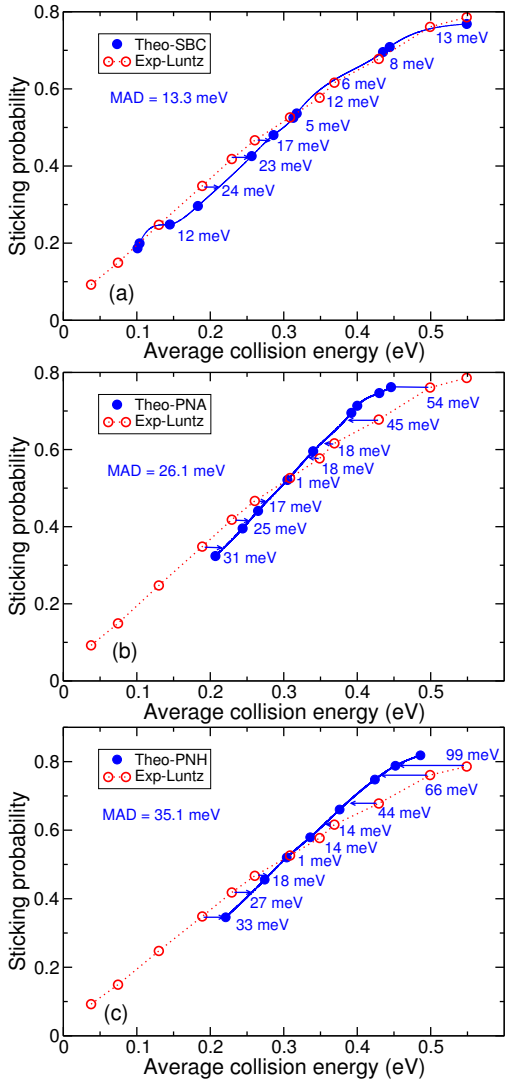

Figure 6.A.2: Comparison of the experimental data from Luntz *et al.* [15], with the theoretical results (a) obtained with the SBC parameters of Cao *et al.* [17], (b) with the PNA [44], and (c) with the PNH parameters of Hodgson and co-workers [36]. In all cases the horizontal arrows and the numbers indicate the energy spacings between the interpolated values of the theoretical results and the actual experimental values. The blue lines show the interpolated curves of the computed data.

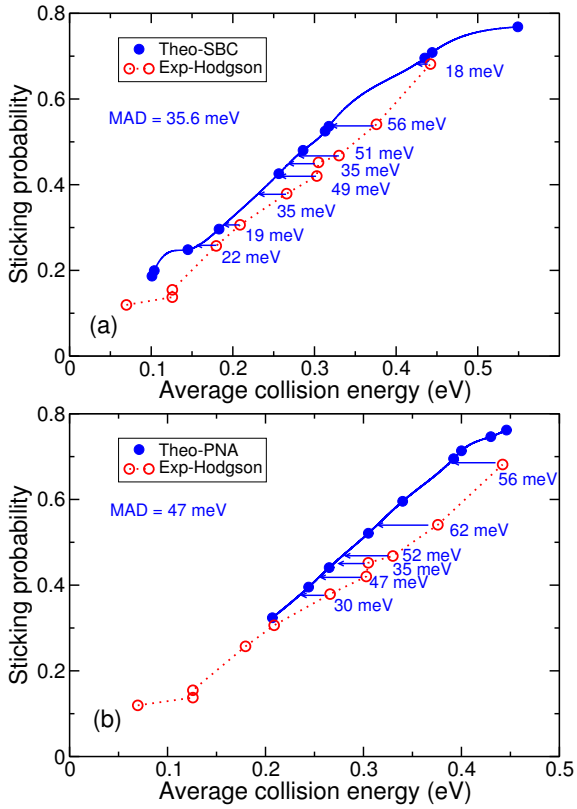

Figure 6.A.3: Comparison of the experimental data from Hodgson *et al.* [16], with the theoretical results (a) obtained with the SBC parameters of Cao *et al.* [17], (b) and with the PNA parameters [44]. In all cases the horizontal arrows and the numbers indicate the energy spacings between the interpolated values of the theoretical results and the actual experimental values. The blue lines show the interpolated curves of the computed data.

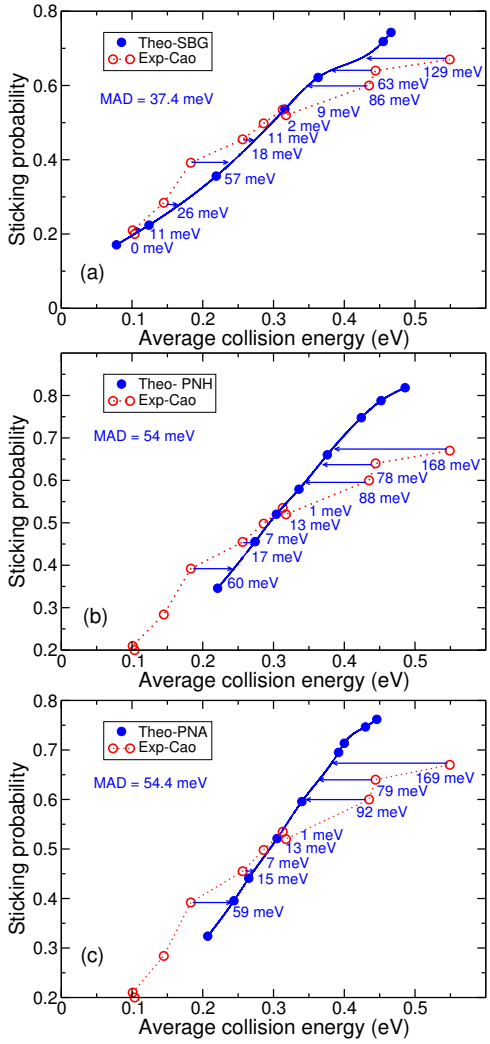

Figure 6.A.4: Comparison of the experimental data from Cao *et al.* [17], with the theoretical results (a) obtained with the SBG parameters of Groot *et al.* [37], (b) with the PNH parameters of Hodgson and co-workers [36], and (c) with the PNA parameters [44]. In all cases the horizontal arrows and the numbers indicate the energy spacings between the interpolated values of the theoretical results and the actual experimental values. The blue lines show the interpolated curves of the computed data.

References

1. Wolcott, C. A., Medford, A. J., Studt, F. & Campbell, C. T. Degree of Rate Control Approach to Computational Catalyst Screening. *Journal of Catalysis* **330,** 197–207 (2015).
2. Sabbe, M. K., Reyniers, M.-F. & Reuter, K. First-Principles Kinetic Modeling in Heterogeneous Catalysis: An Industrial Perspective on Best-Practice, Gaps and Needs. *Catalysis Science & Technology* **2,** 2010–2024 (2012).
3. Noyori, R. Synthesizing Our Future. *Nature Chemistry,* 5–6 (2009).
4. Ertl, G. Primary Steps in Catalytic Synthesis of Ammonia. *Journal of Vacuum Science & Technology A* **1,** 1247–1253 (1983).
5. Chorkendorff I. Niemantsverdriet, J. W. *Concepts of Modern Catalysis and Kinetics.* 452 (Student Edition ed.; Wiley-VCH Verlag GMBH& Co.: Weinheim, Introduction to surface chemistry and catalysis, 2003).
6. Stegelmann, C., Andreasen, A. & Campbell, C. T. Degree of Rate Control: How Much the Energies of Intermediates and Transition States Control Rates. *Journal of the American Chemical Society* **131,** 8077–8082 (2009).
7. Díaz, C. *et al.* Chemically Accurate Simulation of a Prototypical Surface Reaction: H_2 Dissociation on Cu(111). *Science* **326,** 832–834 (2009).
8. Sementa, L. *et al.* Reactive Scattering of H_2 from Cu(100): Comparison of Dynamics Calculations Based on the Specific Reaction Parameter Approach to Density Functional Theory with Experiment. *Journal of Chemical Physics* **138** (2013).
9. Ghassemi, E. N., Wijzenbroek, M., Somers, M. F. & Kroes, G. J. Chemically Accurate Simulation of Dissociative Chemisorption of D_2 on Pt(111). *Chemical Physics Letters* **683.** Ahmed Zewail (1946-2016) Commemoration Issue of Chemical Physics Letters, 329–335 (2017).
10. Nattino, F. *et al.* Chemically Accurate Simulation of a Polyatomic Molecule-Metal Surface Reaction. *Journal of Physical Chemistry Letters* **7,** 2402–2406 (2016).
11. Migliorini, D. *et al.* Surface Reaction Barriometry: Methane Dissociation on Flat and Stepped Transition-Metal Surfaces. *Journal of Physical Chemistry Letters* **8,** 4177–4182 (2017).

12. Boereboom, J. M., Wijzenbroek, M., Somers, M. F. & Kroes, G. J. Towards a Specific Reaction Parameter Density Functional for Reactive Scattering of H_2 from Pd(111). *Journal of Chemical Physics* **139** (2013).

13. Wijzenbroek, M. & Kroes, G. J. The Effect of the Exchange-Correlation Functional on H_2 Dissociation on Ru(0001). *Journal of Chemical Physics* **140** (2014).

14. D. Navalikhina, M. & V. Krylov, O. Heterogeneous Catalysts of Hydrogenation. *Russian Chemical Review* **67,** 587–616 (1998).

15. Luntz, A. C., Brown, J. K. & Williams, M. D. Molecular Beam Studies of H_2 and D_2 Dissociative Chemisorption on Pt(111). *Journal of Chemical Physics* **93,** 5240–5246 (1990).

16. Samson, P., Nesbitt, A., Koel, B. E. & Hodgson, A. Deuterium Dissociation on Ordered Sn/Pt(111) Surface Alloys. *Journal of Chemical Physics* **109,** 3255–3264 (1998).

17. Cao, K., van Lent, R., Kleyn, A. & Juurlink, L. A Molecular Beam Study of D_2 Dissociation on Pt(111): Testing SRP-DFT Calculations. *Chemical Physics Letters* **706,** 680–683 (2018).

18. Cowin, J. P., Yu, C., Sibener, S. J. & Hurst, J. E. Bound Level Resonances in Rotationally Inelastic HD/Pt (111) Surface Scattering. *Journal of Chemical Physics* **75,** 1033–1034 (1981).

19. Cowin, J. P., Yu, C., Sibener, S. J. & Wharton, L. HD Scattering from Pt(111): Rotational Excitation Probabilities. *Journal of Chemical Physics* **79,** 3537–3549 (1983).

20. Cowin, J. P., Yu, C.-F. & Wharton, L. HD Scattering from Pt(111): Rotationally Mediated Selective Adsorption. *Surface Science* **161,** 221–233 (1985).

21. Nieto, P. *et al.* Reactive and Nonreactive Scattering of H_2 from a Metal Surface Is Electronically Adiabatic. *Science* **312,** 86–89 (2006).

22. Halstead, D. & Holloway, S. Quantum-Mechanical Scattering of H_2 from Metal Surfaces: Diffraction and Dissociative Adsorption. *Journal of Chemical Physics* **88,** 7197–7208 (1988).

23. Darling, G. R. & Holloway, S. The Role of Parallel Momentum in the Dissociative Adsorption of H_2 at Highly Corrugated Surfaces. *Surface Science* **304,** L461–L467 (1994).

24. Pijper, E. *et al.* Six-Dimensional Quantum Dynamics of Scattering of (v=0, j=0) H_2 from Pt(1 1 1): Comparison to Experiment and to Classical Dynamics Results. *Chemical Physics Letters* **347,** 277–284 (2001).

25. Pijper, E., Kroes, G. J., Olsen, R. A. & Baerends, E. J. Reactive and Diffractive Scattering of H_2 from Pt(111) Studied Using a Six-Dimensional Wave Packet Method. *Journal of Chemical Physics* **117,** 5885–5898 (2002).

26. Kingma, S. M. *et al.* Diffractive and reactive scattering of (v=0,j=0) HD from Pt(111): Six-dimensional quantum dynamics compared with experiment. *Journal of Chemical Physics* **118,** 4190–4197 (2003).

27. Vincent, J., Olsen, R., Kroes, G. J. & Baerends, E. Dissociative Chemisorption of H_2 on Pt(1 1 1): Isotope Effect and Effects of the Rotational Distribution and Energy Dispersion. *Surface Science* **573,** 433–445 (2004).

28. Ludwig, J. & Vlachos, D. G. *Ab Initio* Molecular Dynamics of Hydrogen Dissociation on Metal Surfaces Using Neural Networks and Novelty Sampling. *Journal of Chemical Physics* **127** (2007).

29. Becke, A. D. Density-Functional Exchange-Energy Approximation with Correct Asymptotic Behavior. *Physical Review A* **38,** 3098–3100 (1988).

30. Perdew, J. P. Density-Functional Approximation for the Correlation Energy of the Inhomogeneous Electron Gas. *Physical Review B* **33,** 8822–8824 (1986).

31. Kroes, G. J., Wijzenbroek, M. & Manson, J. R. Possible Effect of Static Surface Disorder on Diffractive Scattering of H_2 from Ru(0001): Comparison Between Theory and Experiment. *Journal of Chemical Physics* **147,** 244705 (2017).

32. Kosloff, R. Time-Dependent Quantum-Mechanical Methods for Molecular Dynamics. *Journal of Physical Chemistry* **92,** 2087–2100 (1988).

33. King, D. A. & Wells, M. G. Reaction Mechanism in Chemisorption Kinetics: Nitrogen on the 100 Plane of Tungsten. *Proceedings of the Royal Society of London A: Mathematical, Physical and Engineering Sciences* **339,** 245–269 (1974).

34. Luntz, A. C. *Personal communication.*

35. Hodgson, A. *Personal communication.*

36. Cottrell, C., Carter, R. N., Nesbitt, A., Samson, P. & Hodgson, A. Vibrational State Dependence of D_2 Dissociation on Ag(111). *Journal of Chemical Physics* **106,** 4714–4722 (1997).

37. Groot, I. M. N., Ueta, H., van der Niet, M. J. T. C., Kleyn, A. W. & Juurlink, L. B. F. Supersonic Molecular Beam Studies of Dissociative Adsorption of H_2 on Ru(0001). *Journal of Chemical Physics* **127,** 244701 (2007).

38. Groot, I. M. N. *Personal communication.*

39. Rettner, C. T., Michelsen, H. A. & Auerbach, D. J. Quantum-State-Specific Dynamics of the Dissociative Adsorption and Associative Desorption of H_2 at a Cu(111) Surface. *Journal of Chemical Physics* **102,** 4625–4641 (1995).

40. Rendulic, K., Anger, G. & Winkler, A. Wide Range Nozzle Beam Adsorption Data for the Systems H_2/Nickel and H_2/Pd(100). *Surface Science* **208,** 404–424 (1989).

41. Gallagher, R. J. & Fenn, J. B. Rotational Relaxation of Molecular Hydrogen. *Journal of Chemical Physics* **60,** 3492–3499 (1974).

42. Nour Ghassemi, E., Somers, M. & Kroes, G. J. Test of the Transferability of the Specific Reaction Parameter Functional for H_2 + Cu(111) to D_2 + Ag(111). *Journal of Physical Chemistry C* **122,** 22939–22952 (2018).

43. Michelsen, H. A. & Auerbach, D. J. A Critical Examination of Data on the Dissociative Adsorption and Associative Desorption of Hydrogen at Copper Surfaces. *Journal of Chemical Physics* **94,** 7502–7520 (1991).

44. Auerbach, D. J. *Personal communication.*

45. Michelsen, H. A., Rettner, C. T., Auerbach, D. J. & Zare, R. N. Effect of Rotation on the Translational and Vibrational Energy Dependence of the Dissociative Adsorption of D_2 on Cu(111). *Journal of Chemical Physics* **98,** 8294–8307 (1993).

46. Juurlink, L. B. F. *Personal communication.*

47. Madsen, G. K. H. Functional Form of the Generalized Gradient Approximation for Exchange: The PBEα Functional. *Physical Review B* **75,** 195108 (2007).

48. Lee, K., Murray, É. D., Kong, L., Lundqvist, B. I. & Langreth, D. C. Higher-Accuracy van der Waals Density Functional. *Physical Review B* **82,** 081101 (2010).

49. Busnengo, H. F., Salin, A. & Dong, W. Representation of the 6D Potential Energy Surface for a Diatomic Molecule Near a Solid Surface. *Journal of Chemical Physics* **112,** 7641–7651 (2000).

50. Karplus, M., Porter, R. N. & Sharma, R. D. Exchange Reactions with Activation Energy. I. Simple Barrier Potential for (H, H_2). *Journal of Chemical Physics* **43,** 3259–3287 (1965).

51. Wijzenbroek, M., Helstone, D., Meyer, J. & Kroes, G. J. Dynamics of H_2 Dissociation on the Close-Packed (111) Surface of the Noblest Metal: H_2 + Au(111). *Journal of Chemical Physics* **145,** 144701 (2016).

52. Sarma, G., Yang, C.-H., Saha, A. K., Parker, D. H. & Wiesenfeld, L. Rotational excitation of HDO and D_2O by H_2: Experimental and theoretical differential cross-sections. *Journal of Chemical Physics* **138** (2013).

53. Kresse, G. & Hafner, J. *Ab Initio* Molecular Dynamics for Liquid Metals. *Physical Review B* **47,** 558–561 (1993).

54. Kresse, G. & Hafner, J. *Ab Initio* Molecular-Dynamics Simulation of the Liquid-Metal-Amorphous-Semiconductor Transition in Germanium. *Physical Review B* **49,** 14251–14269 (1994).

55. Kresse, G. & Furthmüller, J. Efficiency of *Ab-Initio* Total Energy Calculations for Metals and Semiconductors Using a Plane-Wave Basis Set. *Computational Materials Science* **6,** 15–50 (1996).

56. Kresse, G. & Furthmüller, J. Efficient Iterative Schemes for *Ab Initio* Total-Energy Calculations Using a Plane-Wave Basis Set. *Physical Review B* **54,** 11169–11186 (1996).

57. Blöchl, P. E. Projector Augmented-Wave Method. *Physical Review B* **50,** 17953–17979 (1994).

58. Román-Pérez, G. & Soler, J. M. Efficient Implementation of a van der Waals Density Functional: Application to Double-Wall Carbon Nanotubes. *Physical Review Letters* **103,** 096102 (2009).

59. Ghassemi, E. N. *et al.* Transferability of the Specific Reaction Parameter Density Functional for H_2 + Pt(111) to H_2 + Pt(211). *Journal of Physical Chemistry C* **123,** 2973–2986 (2019).

60. Pijper, E., Kroes, G. J., Olsen, R. A. & Baerends, E. J. Dissociative and Diffractive Scattering of H_2 from Pt(111): A Four-Dimensional Quantum Dynamics Study. *Journal of Chemical Physics* **116,** 9435–9448 (2002).

61. Díaz, C., Olsen, R. A., Busnengo, H. F. & Kroes, G. J. Dynamics on Six-Dimensional Potential Energy Surfaces for H_2/Cu(111): Corrugation Reducing Procedure versus Modified Shepard Interpolation Method and PW91 versus RPBE. *Journal of Physical Chemistry C* **114,** 11192–11201 (2010).

62. Kroes, G. J. & Díaz, C. Quantum and Classical Dynamics of Reactive Scattering of H_2 from Metal Surfaces. *Chemical Society Reviews* **45,** 3658–3700 (2016).

63. Chow, H. & Thompson, E. The Optical Potential in the Scattering of Hydrogen and Deuterium Atoms from LiF and NaF(001)*. *Surface Science* **82,** 1–21 (1979).